Low-Temperature-Induced Structural Changes in Human Lysozyme Elucidated by Three-Dimensional NMR Spectroscopy‡

Hiroyuki Kumeta,[§,||] Ai Miura,[§] Yoshihiro Kobashigawa,[§,||] Kazunori Miura,[§] Chitoshi Oka,[⊥] Nobuaki Nemoto,[#] Katsutoshi Nitta,[||] and Sakae Tsuda*[,§]

Protein Structure Research Group, Institute for Biological Resources and Functions, National Institute of Advanced Industrial Science and Technology (AIST), 2-17-2-1, Tsukisamu-Higashi, Toyohira, Sapporo 062-8517, Japan, Division of Biological Sciences, Graduate School of Science, Hokkaido University, N10W8, Kita-ku, Sapporo 060-0810, Japan, Chiba Prefectural Industrial Research Institute, 889 Kasori, Wakaba, Chiba 264-0017, Japan, and Varian Japan, Varian Japan Sumitomo Shibaura Building, 4-16-36 Shibaura, Minato-ku, Tokyo 108-0023, Japan

Received September 5, 2002; Revised Manuscript Received November 22, 2002

ABSTRACT: The three-dimensional solution structures of human lysozyme were determined at 35 and 4 °C using the heteronuclear multidimensional NMR spectroscopy, which were compared with each other to clarify the structural response of this enzyme to lowering of the temperature. Together with the data of the temperature dependence experiments of the lytic activity against *Micrococcus luteus*, we consider the implication of the observed structural change for the low-temperature-induced reduction of the activity of human lysozyme. The structures of human lysozyme determined at the two temperatures are found to be similar, both of which comprise four α-helices (A- to D-helices) and three antiparallel β-strands ($\beta_1-\beta_3$), leading to the constructions of the α- and β-domains as previously identified in the X-ray crystal structure. A significant structural change was observed for the "active site lobe" comprising the loop region connecting C- and D-helices and the following D-helix, which moves toward the active site cleft located between the α- and β-domains so as to obstruct the cleft according to the temperature lowering. It further appeared that the total volume as well as the accessible surface area of human lysozyme decreases with lowering of the temperature, suggesting that the internal cavity of this enzyme shrinks under low temperature environment. Because in human lysozyme the region comprising the active site lobe is responsible for turnover of the enzymatic reaction against the substrate, the low-temperature-induced structural change of the active site lobe presumably controls the efficiency of the lytic activity under low temperatures.

An enzymatic activity is generally depressed by decreasing of the temperature from the optimum point to the freezing point (0 °C). The inclination of the relative activity between the two points is correlated with the activation energy of the enzymatic reaction, which is generally small for the so-called psychrophilic enzyme if compared with the mesophilic counterparts. Because such a maintained catalytic activity even under cold temperature possesses a significant importance for industrial usages, the structural characteristics essential for such enzyme have been studied extensively (*1*−*3*), which commonly pointed out that a flexible functional region is one of the key determinants to provide a significant activity under cold temperature. This evoked us a question about whether a functional region of a certain protein specifically shows a structural response to lowering of the temperature under nondenatured conditions. In the case of the regulatory N-domain of troponin C (NTnC),[1] we previously determined the NMR solution structures at 30 and 4 °C; the comparison between them clearly revealed that a specific change occurs for a flexible functional region accompanying a local structural change at "hinge" residues with decreasing of the cavity volume of the protein (*4*). Although for several model proteins the low-temperature-induced shrinkage in the cavity volume has been identified (*5*), it is still unknown for many proteins whether their functional region specifically acquires a structural ability to respond to lowering of the temperature, especially in the case of enzyme. The NMR spectroscopy clarifies the low-temperature-induced change of the three-dimensional (3D) structure and dynamics of an enzyme at the per residue level, which is thought to provide crucial information to design and produce an activity-enhanced mutant or artificially modified protein that acts even under a cold environment.

‡ The atomic coordinates for the final structures and the sets of restraints have been deposited with the Brookhaven Protein Data Bank (accession codes 1IY4 for 35 °C and 1IY3 for 4 °C minimized average structure).

* To whom correspondence should be addressed. E-mail: sakae.tsuda@aist.go.jp. Phone: +81-11-857-8912. Fax: +81-11-857-8983.

§ National Institute of Advanced Industrial Science and Technology.

|| Hokkaido University.

⊥ Chiba Prefectural Industrial Research Institute.

Varian Japan.

[1] Abbreviations: NTnC, N-domain of troponin C; 2D and 3D, two and three dimensional; NAG, *N*-acetylglucosamine; T_1, longitudinal relaxation time; T_2, transverse relaxation time; NOE, nuclear Overhauser enhancement effect; HSQC, heteronuclear single-quantum coherence spectroscopy; DSS, 2,2-dimethyl-2-silapentane-5-sulfonate sodium salt; τ_m, overall rotational correlation time; τ_e, internal rotational correlation time; S^2, generalized order parameter; R_{ex}, exchange contribution to line shape; rmsd, root-mean-square distance.

10.1021/bi026730w CCC: $25.00
Published on Web 01/17/2003

Here we choose human lysozyme (130 residues, MW = 14300) as a model enzyme to monitor the low-temperature-induced change using homo- and heteronuclear multidimensional NMR techniques. Lysozyme is well-known to hydrolyze either the β-(1−4)-linked homopolymer of *N*-acetylchitose (chitin) or the β-(1−4)-linked alternative copolymer composed of *N*-acetylchitose and *N*-acetylmuramic acid in the peptidoglycan component of the cell walls of Gram-positive bacteria (*6*, *7*). A large body of the structural database of the lysozyme family is currently available, which includes the X-ray crystal structure of human lysozyme at 1.5 Å resolution (*8*). Human lysozyme comprises four α-helices [A-helix (residues Arg^{5}−Arg^{14}), B-helix (Leu^{25}−Glu^{35}), C-helix (Ala^{90}−Val^{99}), and D-helix (Val^{110}−Cys^{116})], three antiparallel β-strands (b_1, Ala^{42}−Asn^{46}; b_2, Ser^{51}−Ile^{56}; and b_3, Ile^{59}−Ser^{61}), and four disulfide bonds (Cys^{6}−Cys^{128}, Cys^{30}−Cys^{116}, Cys^{64}−Cys^{81}, and Cys^{77}−Cys^{95}), which construct the α-helix-rich and β-strand-rich domains (named α- and β-domains), as typically identified for all of the chicken-type (C-type) lysozyme (*9*). The structure of human lysozyme cocrystallized with a substrate analogue (hexa-*N*-acetylchitohexaose) has also been solved (*10*), which demonstrated that an active site cleft was located between the α- and β-domains. The residues lining in the globular-shaped cleft can accommodate its targeting six oligosaccharide units in the sites generally termed subsites A−F (*11*), which include Thr^{43}, Asn^{44}, Asn^{46}, Thr^{52}, and Ile^{56}−Ile^{59} located in the β-sheet, the C-terminus of the B-helix (Trp^{34}−Ser^{36}), the loop connecting the C- and D-helices (residues Arg^{98} and Arg^{101}−Pro^{103}), the N-terminus of the D-helix (residues Arg^{107}−Val^{110} and Trp^{112}), and residues Arg^{62}, Tyr^{63}, and Ala^{73}. The structural database also includes the X-ray structure of a C-type lysozyme from fish rainbow trout crystallized at 4 °C (*12*, *13*), which shares 68% amino acid homology with human lysozyme. Below 20 °C, the rainbow trout lysozyme possesses lower activation energy for catalytic activity against *Micrococcus luteus* than hen egg white lysozyme, so that this fish lysozyme was assumed to be one of the cold-adapted variants (*14*). Hence, it might be interesting to consider the structural response of human lysozyme to lowering of the temperature with regard to the structural characteristics of rainbow trout lysozyme.

The ^{1}H and ^{15}N NMR spectral assignments have been performed for human lysozyme without substrate at temperatures of 35 °C (*15*, *16*) and of 40 °C (*17*). For human lysozyme complexed with a substrate analogue, tri-*N*-acetylchitotrioside denoted as $(NAG)_3$, Mine et al. (*16*) made the complete NMR assignments and executed the ^{15}N NMR relaxation measurements (i.e., T_1, T_2, and NOE) so as to elucidate the $(NAG)_3$-binding effect on the motions of the backbone NH bond vectors in the pico- to millisecond time scale. This dynamical analysis was performed by application of the model-free formalism of the spectral density function (*18*, *19*) and by assuming the isotropic overall rotation of the molecule, which gave significant information about the detailed dynamic behavior of human lysozyme. Mine et al. (*16*) revealed that, for example, only folding pattern is the major determinant for the internal backbone motions of human lysozyme, and the difference in internal motion in the lobe composed of residues Val^{100}−Arg^{115} in lysozyme may be involved in the improvement of the activity. Interestingly, the NMR-based solution structure has been determined only for hen egg white lysozyme at 35 °C (*20*; PDB code 1E8L) and for canine milk lysozyme at 30 °C (PDB code 1I56) among all of the members of lysozyme family, one reason of which may be due to the lack of a high-level secretion system of human lysozyme. Recently, Oka et al. (*21*) established such a system for human lysozyme using *Pichia pastoris*, which enabled us to overexpress the ^{15}N-labeled and the $^{13}C/^{15}N$-doubly labeled proteins efficiently. On the basis of the complete assignments of the ^{1}H, ^{15}N, and ^{13}C resonances at 35 and 4 °C (*22*), here we succeeded in determining the NMR solution structures at each temperature. Together with our ^{15}N NMR backbone dynamics measurement at 4 °C, we will discuss the structural and dynamical response of human lysozyme to lowering of the temperature and the implications for the low-temperature-induced depression of the catalytic activity.

EXPERIMENTAL PROCEDURES

Sample Preparation. The expression system and purification method of human lysozyme were reported as described previously (*21*). The ^{15}N-labeled human lysozyme was obtained from the MM medium [1.34% yeast nitrogen base without $(NH_4)_2SO_4$, (4×10^{-5})% biotin, 0.5% methanol] containing the ^{15}N-labeled $(NH_4)_2SO_4$. For the ^{13}C-labeling, we used ^{13}C-labeled methanol as a carbon source. The sample was concentrated by ultrafiltration using Centriprep-10 (Millipore) and then lyophilized. The NMR sample was prepared by dissolving 2 mM lyophilized human lysozyme in 0.5 mL of H_2O containing 50 mM KCl and 10% D_2O for the lock. The final pH of the sample was adjusted to 3.8 by additions of small aliquots of either DCl or KOD.

Measurement of Enzymatic Activity. The lytic activity of human lysozyme against *M. luteus* was measured photometrically by a modification of the method by Morsky (*23*). The assay sample (200 μL) was added to 800 μL of a cell suspension of *M. luteus* (0.15 mg/mL) in 50 mM sodium phosphate buffer (pH 6.4). The bacteriolytic activity was estimated from the slope in the absorbance at 450 nm for 3 min after addition of human lysozyme.

NMR Spectroscopy. All NMR spectra were obtained using a Varian Unity INOVA 500 MHz spectrometer equipped with triple resonance probe heads and *x*-, *y*-, *z*-axis pulsed field gradients. For the assignments of ^{1}H, ^{13}C, and ^{15}N resonances, the following multidimensional NMR experiments were carried out: ^{15}N-HSQC (*24*), ^{13}C-HSQC (*25*), CBCA(CO)NNH (*26*), HNCACB (*27*), C(CO)NH (*28*), H(CCO)NH (*28*), ^{15}N-edited NOESY (75 ms mixing time) (*29*), ^{15}N-edited TOCSY (*30*), and ^{13}C-edited NOESY (*31*). The 3D-HNHA (*32*) experiments were performed to obtain the ^{3}J coupling constants between NH and the $C_\alpha H$ proton. The set of NMR spectra was acquired at both 35 and 4 °C. The ^{1}H chemical shifts were referenced from 2,2-dimethyl-2-silapentane-5-sulfonate sodium salt (DSS). The ^{13}C and ^{15}N chemical shifts were referenced indirectly from internal DSS as previously described (*33*). All of the NMR data were processed and analyzed on a SGI O^2 workstation (Silicon Graphics, Mountain View, CA) using NMRPipe (*34*) and PIPP (*35*) software. The complete assignment of ^{1}H, ^{13}C, and ^{15}N resonances of human lysozyme at both temperatures was reported (*22*) and deposited in the BioMagResBank database (http://www.bmrb.wisc.edu).

Table 1: Statistics of the 20 Solution Structures of Human Lysozyme at 35 and 4 °C

	35 °C	4 °C
no. of distance restraints		
totals	1676	1774
intraresidue	741	778
sequential	422	524
medium range ($\|i-j\| \leq 4$)	211	217
long range ($\|i-j\| > 4$)	302	260
dihedral restraints (ϕ)	96	63
distance restraint violation (>0.1 Å)	0	2
backbone atoms rmsd (Å^2)	0.865	0.835
energies (kcal/mol)		
F_{total}	163.08 ± 6.67	153.88 ± 3.31
F_{bonds}	3.77 ± 0.45	3.20 ± 0.28
F_{angles}	128.56 ± 3.56	123.10 ± 2.05
$F_{impropers}$	18.58 ± 0.51	17.90 ± 0.40
$F_{van\ der\ Waals}$	8.36 ± 2.45	6.32 ± 1.06
F_{NOE}	3.66 ± 1.06	3.27 ± 0.62
ϕ and ψ in allowed region (%)	99.9	99.5

Structural Determination. Interproton distance restraints were obtained from ^{15}N-edited NOESY and ^{13}C-edited NOESY with the lower bound on all proton−proton restraints setting to 1.7 Å. The hydrogen-bonding restraints obtained using the hbplus program (*36*) were set to 1.8 ± 0.5 Å for the HN−O distances and 2.8 ± 0.5 Å for the N−O distances. Backbone ϕ dihedral angle restraints were based on the Karplus equation: $^3J_{NHHa} = 6.51 \cos^2(\phi - 60°) - 1.76 \cos(\phi - 60°) + 1.60$ (*32*). The minimum restraint range was set to ±20°. In the initial calculation stage, 100 starting structures from an extended conformation of human lysozyme were calculated by using the simulated annealing (SA) protocol of X-PLOR 3.851 (*37*) with heating for 60 ps and cooling for 30 ps. Approximately 70% of the initial structures were converged. The type and number of distance and dihedral restraints are summarized in Table 1. The structural refinement was carried out by starting with the 50 lowest energy converged structures using the X-PLOR SA protocol by applying the NOE restraints plus the hydrogen-bonding and ϕ-angle restraints with heating for 30 ps and cooling for 20 ps. The VADAR (D. S. Wishart, L. Willard, and B. D. Sykes, unpublished) and PROCHECK (*38*) programs were also used to identify the well-defined secondary structural elements from the 20 lowest total energy structures, and ϕ-angle restraints were applied for subsequent rounds of the refinement. The energy-minimized average structure at both temperatures was calculated from the 20 lowest total energy structures using the SA protocol with the following steps: (i) 2000 cycles of restrained energy minimization and (ii) 800 cycles of unrestrained energy minimization. All structure calculation was performed on a SGI O^2 workstation. The Molscript (*39*), Raster 3D (*40*), and MOLMOL (*41*) programs were used for structural descriptions.

Backbone Amide ^{15}N Relaxation Measurement. The ^{15}N relaxation measurements (^{15}N−T_1, ^{15}N−T_2, and ^{1}H−^{15}N NOE) were performed on a Varian Unity INOVA 500 spectrometer at 35 and 4 °C using the pulse sequences described in ref *42*. T delays were used for T_1 (T = 0, 10, 20, 40, 80, 160, 320, and 640 ms) and T_2 (T = 10, 30, 50, 70, 90, 110, 130, and 150 ms). The decays of cross-peak intensities with time T in the T_1 and T_2 experiments were fitted to a single exponential by a nonlinear least-squares method. All of the ^{1}H−^{15}N two-dimensional (2D) spectra were peak-picked using the PIPP program. The steady-state ^{1}H−^{15}N NOE values were determined from the ratio of the intensities of the peaks with and without proton saturation. Peak intensity was estimated by using the PIPP program. We employed the following three spectral density models for fitting of the obtained ^{15}N relaxation data: (i) the simple S^2−τ_e model, (ii) the S^2−τ_e−R_{ex} model where the additional R_{ex} term takes into account potential chemical or conformational exchange, and (iii) the two-time-scale S_s^2−S_f^2−τ_s model where S_s^2 and S_f^2 are the order parameters characterizing the slow and fast internal motions, respectively. We found the best-fit sets of the model-free motional parameters (S^2, τ_e, R_{ex}, S_s^2, and S_f^2) using our in-house grid search program, which optimizes the χ^2 function given by Farrow et al. (*43*).

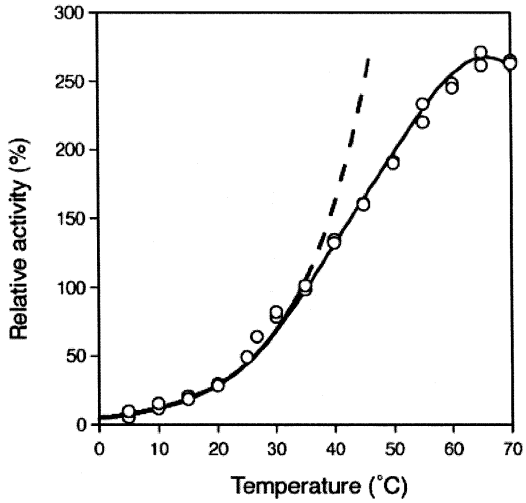

FIGURE 1: Temperature dependence of the lytic activity of human lysozyme against *M. luteus*. The activity was plotted as a function of temperature from 4 to 70 °C, for which the activity at 35 °C is standardized to be 100%.

RESULTS

Enzymatic Activity. Figure 1 shows the lytic activity of human lysozyme against *M. luteus* measured in the temperature range between 4 and 70 °C, for which the activity at 35 °C is standardized to be 100%. As shown, human lysozyme exhibits an ordinary profile of thermal dependence of the enzymatic activity, which is theoretically assumed to be a summation of the exponential and the bell-shaped curves, the former originating from the noncatalyzed reaction and the latter originating from irreversible denaturation (*44*). As for Figure 1, the exponential part of the curve (guided by broken lines) reflects the genuine thermal dependence of the chemical reaction, and the part of the curve between almost midpoint of the slope and the top region arises from the balance between heat-induced activation and thermal unfolding states. Consequently, we could evaluate the optimum temperature of 63 °C and the activation energy of 41.8 kJ K^{-1} mol^{-1} (using Arrhenius plot) for the catalytic activity of human lysozyme. When the relative activity of human lysozyme at 4 °C is compared with the value at 35 °C, the reduction ratio (4 °C/35 °C) is 7.6%. These evaluations are nearly identical to that evaluated for the other C-type lysozyme including hen egg white lysozyme and canine milk lysozyme using the same substrate (10.8% and 11.8%, respectively). The human lysozyme exhibits 60.2%

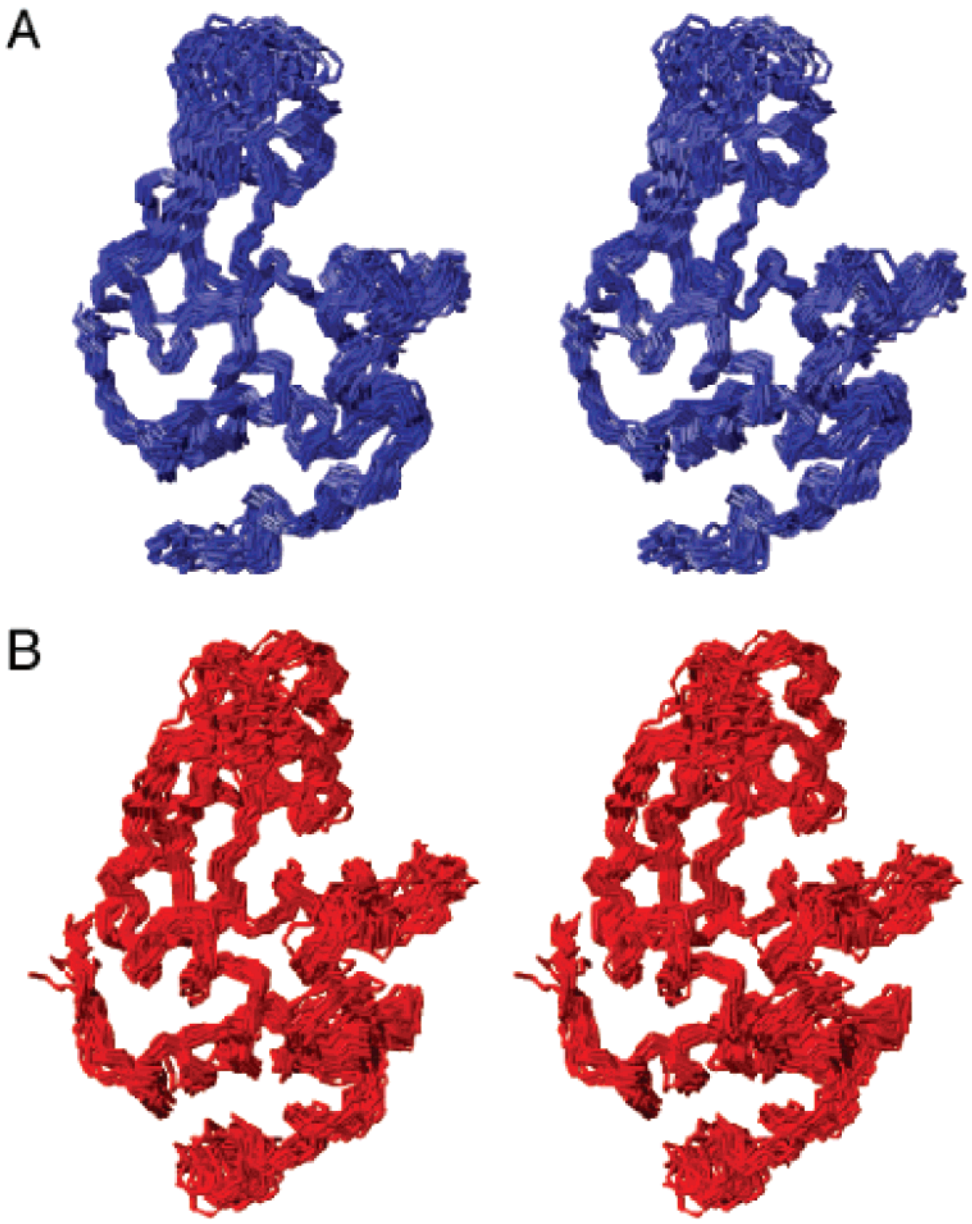

FIGURE 2: Stereoviews of the solution structures of human lysozyme determined at 4 °C (A, blue) and at 35 °C (B, red). For each structure, the backbone atoms (N, C_α, and C′) of the family of 20 structures are well superimposed and shown in the rod representations. Only two loop regions (residues Ala^{47}−Arg^{50} and Lys^{68}−Gly^{72}) and the C-terminal region (Val^{125}−Val^{130}) are poorly defined presumably due to their high segmental mobility. This figure was produced with the program MOLMOL (*41*).

sequence homology with the hen egg white lysozyme, 51.5% homology with canine milk lysozyme, and 68.5% homology with the rainbow trout lysozyme, respectively. It should be noted that only below 20 °C the lytic activity of rainbow trout lysozyme is significantly higher than that of the hen egg white lysozyme (*14*). It has been demonstrated that these lysozymes construct a highly homologous three-dimensional structure comprising the same sets of the secondary structural components. These data indicate that the C-type lysozymes possess a similar, but not identical temperature dependence of the lytic activity irrespective of their amino acid replacements.

Structural Determination of Human Lysozyme at 35 and 4 °C. On the basis of the complete assignments of the ^1H, ^{15}N, and ^{13}C resonances performed at 35 and 4 °C, the solution structures of human lysozyme were determined at these two temperatures using the NMR-derived 1772 and 1837 experimental restraints, respectively. For each structure, we obtained a total of 1676 and 1774 NOEs, of which 741 and 778 are intraresidual ($|i - j| = 0$), 211 and 217 are medium-range ($1 \leq |i - j| \leq 4$), and 302 and 260 are long-range NOEs ($|i - j| \geq 5$), respectively, where i and j are the residue numbers of two atoms. Totals of 96 (35 °C) and 63 (4 °C) dihedral ϕ angle restraints were obtained from the measurements of the $^3J_{NH-Ha}$ coupling constants by using 3D-HNHA experiments. Statistics of the structural calculation are listed in Table 1. The 20 calculated structures for both temperatures have no distance violation greater than 0.2 Å. Panels A and B of Figure 2 show the well-converged 20 structures determined at 4 and 35 °C, respectively, both of which are superimposed on the residues from Arg^5 to Val^{125}. The root-mean-square distance (rmsd) of the heavy backbone atoms (C_α, C′, and N) of the converged structures against the average minimized structure is 0.865 Å at 35 °C and 0.835 Å at 4 °C, respectively. The Ramachandran plot was obtained with the PROCHECK program. It revealed that

Table 2: Segmental rmsd (Å) between the 35 °C, 4 °C, and X-ray Structures

	segment	35−4 °C	X-ray−35 °C	X-ray−4 °C
A-helix	Arg^{5}−Arg^{14}	0.228	0.118	0.164
B-helix	Leu^{25}−Glu^{35}	0.255	0.247	0.204
C-helix	Ala^{90}−Val^{99}	0.265	0.221	0.130
D-helix	Val^{110}−Cys^{116}	0.264	0.250	0.122
β-sheet	Ala^{42}−Asn^{46}, Ser^{51}−Ile^{56}, Ile^{59}−Ser^{61}	0.589	0.448	0.377

99.9% (35 °C) and 99.5% (4 °C) of the ϕ and ψ angles fall into the allowed region except for glycines, which validate the qualities of the present determined structures.

It appeared that the secondary structural locations of human lysozyme are not significantly different between the 35 °C, 4 °C, and the X-ray crystal structures (*8*). The solution structures are found to comprise two distinct domains: the α-helix-rich domain (denoted as α-domain, residue numbers Lys^{1}−Thr^{40} and Ala^{90}−Val^{130}) and the β-strand-rich domain (β-domain, Arg^{41}−Ile^{89}). The locations of four α-helices and three β-strands identified in the two NMR structures are A-helix (Arg^{5}−Arg^{14}), B-helix (Leu^{25}−Glu^{35}), C-helix (Ala^{90}−Val^{99}), D-helix (Val^{110}−Cys^{116}), β_1-strand (Ala^{42}−Asn^{46}), β_2-strand (Ser^{51}−Ile^{56}), and β_3-strand (Ile^{59}−Ser^{61}). Poorly defined regions are the two loop regions (residues Ala^{47}−Arg^{50} and Lys^{68}−Gly^{72}) and the C-terminal region (Val^{125}−Val^{130}), which are known to exhibit higher segmental motions in the members of lysozyme family as suggested by the ^{15}N NMR relaxation measurement (*16*). The high segmental motions for these regions were also suggested by the X-ray study (*8*) and a recent high-resolution solution structure determined using the NMR residual dipolar coupling information (*20*). When it compared the overall structure between the X-ray crystal structure (denoted X-ray), the 35 °C solution structure (35-NMR), and the 4 °C solution structure (4-NMR), the backbone rmsd evaluated for a segment Arg^{5}−Gln^{126} between X-ray and 35-NMR is 0.926 Å, X-ray and 4-NMR is 0.670 Å, and 35-NMR and 4-NMR is 0.830 Å, respectively. The backbone rmsd for the α-helical regions except for the D-helix (residues Arg^{5}−Tyr^{38} and Ala^{90}−Val^{99}) between the X-ray and 35 °C NMR is 0.342 Å, the X-ray and 4 °C NMR is 0.366 Å, and the 35 °C NMR and 4 °C NMR is 0.410 Å, respectively. The segmental rmsd are also listed in Table 2. These data imply that the overall structural feature of human lysozyme is not changed by dissolving in water and by lowering of the temperature from 35 to 4 °C.

Structural Change of Human Lysozyme by Temperature Lowering. Figure 3A shows the minimized average structures of human lysozyme determined at 35 and 4 °C, which are superimposed so as to achieve the smallest rmsd of the two coordinates. The differences for the backbone coordinates of the two structures are plotted in Figure 3B, for which the secondary structures are depicted along the residual numbers. Taking into account an uncertainty of the NMR-based protein structures, the two coordinates are thought to be identical for most of the region within the range of about 2 Å. It appeared that a loop connecting the β1 and β2 strands (i.e., Asn^{46}−Ser^{51}) exhibits a significant difference in coordinate larger than 2 Å (Figure 3B). Again this region is poorly defined in all of the available coordinates of lysozyme, which

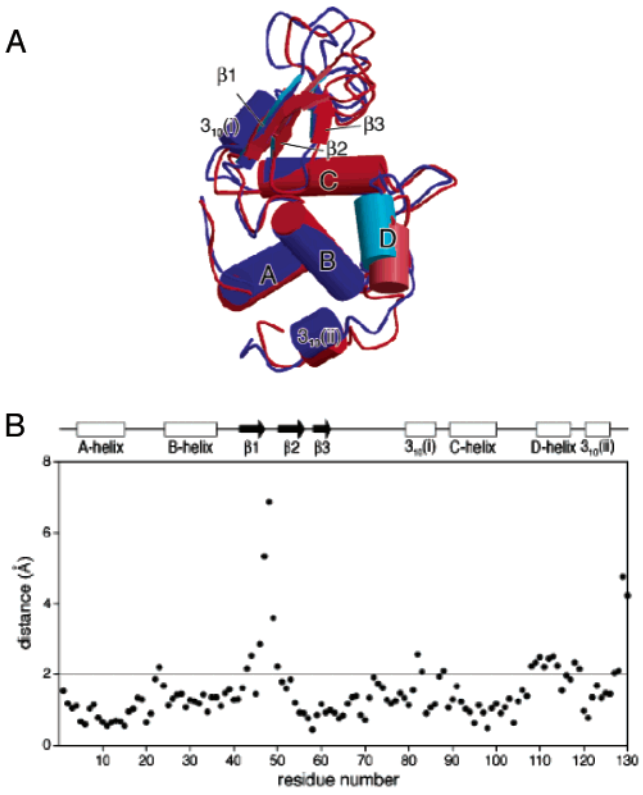

FIGURE 3: (A) Comparison of the structure of human lysozyme determined at 4 °C (blue) with that determined at 35 °C (red). The cylinders represent the secondary structural components of the A- to D-helices as well as the 3_{10}-helices, and the arrows represent those of the β-strands. A significant change of the structure was observed for a region including the D-helix (4 °C, light blue; 35 °C, pink). This figure was produced with the programs Molscript (*39*) and Raster3D (*40*). (B) Difference in the backbone coordinates (Å) of human lysozyme between 4 and 35 °C. The secondary structural components are depicted along the amino acid sequence.

Table 3: Comparison of Interhelical Angles, Accessible Surface Area, and Total Volume of Human Lysozyme between 35 and 4 °C

	35 °C	4 °C
interhelical angles (deg)		
A B	126 ± 4	130 ± 3
A C	79 ± 4	72 ± 3
A D	117 ± 7	119 ± 6
B C	100 ± 4	110 ± 2
B D	117 ± 6	110 ± 4
C D	97 ± 5	84 ± 3
total volume (Å^3)	14923 ± 452	14262 ± 381
accessible surface area (Å^2)	6835 ± 155	6676 ± 98

is ascribable to its higher segmental mobility. Another region showing a significant difference is the N-terminal side of the D-helix (Figure 3), the orientational change of which presumably leads to the difference in coordinate of the following C-terminal segment (Figure 3B). The structural change of the D-helix is characterized as the 13° change of the interhelical angles between C- and D-helices as listed in Table 3. This specific low-temperature-induced change presumably correlates with the reductions of the total volume as well as the accessible surface area with decreasing of the temperature. The total volume of 14923 Å^3 and the accessible surface area of 6835 Å^2 are estimated for the intact molecule (Cys^{6}−Val^{125}) of the 35 °C NMR structure and those of 14262 Å^3 and 6677 Å^2 estimated for the same region of the 4 °C structure on the assumption that the molecule is

spherical in shape (program VADAR) (Table 3). For the region from Cys^6 to Trp^{109} that lacks the D-helix, the total volumes of 12513 Å^3 and 11607 Å are estimated for the 35 and 4 °C structures, respectively. These data show that 5−7% of the total volume of human lysozyme decreases by lowering of the temperature from 35 to 4 °C, which is in accordance with the result of adiabatic compressibility experiments (5).

Backbone Dynamics at 35 and 4 °C. The ^{15}N NMR relaxation data (i.e., T_1, T_2, and NOE) of the backbone NH bond vectors were obtained for 121 and 107 amide groups at 35 and 4 °C, respectively, which gave nonoverlapping ^{15}N-HSQC cross-peaks. For these residues, on-average values of T_1 = 411.3 ms, T_2 = 144.5 ms, and NOE = 0.65 are estimated for 35 °C, and those of T_1 = 763.0 ms, T_2 = 66.0 ms, and NOE = 0.74 are estimated for 4 °C, respectively. For ligand-free and -bound human lysozymes, Mine et al. (*16*) closely examined the ^{15}N internal dynamics at 35 °C (pH = 3.8) on the basis of the assumption that the relaxation is principally governed by the isotropic rotational diffusion. The present data were analyzed under the same assumption using the Lipari−Szabo model-free formalism (*18*, *19*), paying our attention to the conformational exchange term (R_{ex}), which is often interpretable to the result of the rotational diffusion anisotropy (*45*, *46*). We applied five types of the model-free spectral density functions as described in Mine et al. (*16*) and optimized them by fitting of the functions to the obtained set of the relaxation parameters. For the first estimation of the overall rotational correlation time (τ_m), we used the T_1/T_2 ratio of each residue whose NOE value is larger than 0.60 (500 MHz), satisfying the condition $\tau_m \ll w_H^{-1}$ (*47*). Consequently, the overall correlation times (τ_m) of 5.2 and 12.9 ns were evaluated for 35 and 4 °C, respectively. The former is comparable to the value of 4.97 ns previously estimated for the ligand-free human lysozyme at 35 °C (pH = 3.8) (*16*). Figure 4A shows the generalized order parameters (S^2) reflecting a piscosecond to nanosecond time scale of internal motion evaluated for ^{15}N-labeled human lysozyme at 35 °C (closed circles) and 4 °C (open circles). As shown, the present obtained S^2 profile at 35 °C is similar to that of Mine et al. (*16*), which verifies the Mine indication that the folded pattern is the major determinant of the internal motion of lysozyme. It obtained a similar profile of S^2 for the 4 °C structure, the on-average value of which (0.879) is slightly higher than that evaluated for 35 °C (0.841). This result suggests that the internal motion of human lysozyme is slightly depressed throughout the molecule with decreasing of the temperature. As shown in Figure 4B, a significant increase of R_{ex} with the temperature lowering was detected for the linker region located at the C-terminal side of β_3 and for the region including the D-helix. Again, the R_{ex} is often interpretable to the result of the rotational diffusion anisotropy (*45*, *46*) and that the change of R_{ex} at the D-helix is presumably a result of the orientational change of the D-helix (Figure 3) of human lysozyme with lowering of the temperature.

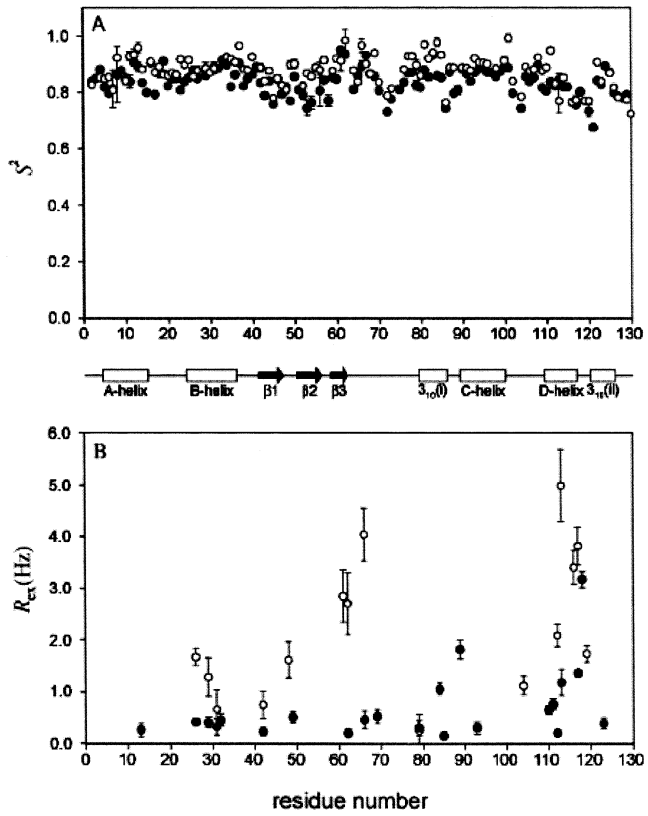

FIGURE 4: (A) Comparison of the generalized order parameter (S^2) of the backbone NH bond vector of human lysozyme at 35 °C (closed circles) with that at 4 °C (open circles), which is extracted from ^{15}N NMR relaxation measurements (T_1, T_2, and NOE). The evaluations are made by fitting of the parameter using the model-free approach (*18*, *19*) under the assumption of isotropic tumbling. (B) R_{ex} term plotted for the residues that require its inclusion in the fitting process. The data obtained at 4 °C are represented by open circles and those at 35 °C by closed circles; the latter is highly identical with the data shown in Figure 3 of Mine et al. (*16*). The secondary structural components are depicted between the plots.

DISCUSSION

The present study characterizes for the first time detailed 3D structural changes of human lysozyme induced by lowering of the temperature under nondenatured conditions. The most significant observation is that residues Ile^{106}−Asp^{120} including the D-helix specifically undergo a structural change with lowering of the temperature (Figure 3) as characterized by the change of the 13° interhelical angle between C- and D-helices (Table 3). This change of residues Ile^{106}−Asp^{120}, which comprises the α-domain's side of the wall of the active site cleft, is depicted in Figure 5 as the GRASP representation (red, 35 °C; blue, 4 °C). This cleft lobe was thought to be responsible for the turnover in the enzymatic reaction (*48*). As shown in Figure 5, this region moves toward the polysaccharide binding cleft (i.e., subsites A−F) by lowering of the temperature from 35 to 4 °C so as to obstruct the cleft. Song et al. (*10*) determined the two X-ray crystal structures of human lysozyme denoted as MOL1 and MOL2 at 1.6 Å resolution; the former constructs a complex with $(NAG)_4$ and $(NAG)_2$, both cleaved from $(NAG)_6$, and the latter with $(NAG)_4$. It appeared that the $(NAG)_4$ is bound to subsites A, B, C, and D, and $(NAG)_2$ also comes closer to subsites E and F. Song et al. (*10*) further made comparisons between the complex and a ligand-free structure determined by Artymiuk and Blake (*8*), which revealed that an almost identical region (Asp^{102}−Asp^{120}) of human lysozyme shows significant shifts of the backbone atom positions when it forms a complex with the ligand. They further recognized that the movement occurs toward the region of residues Cys^{30}−Thr^{70}, which results in "closing"

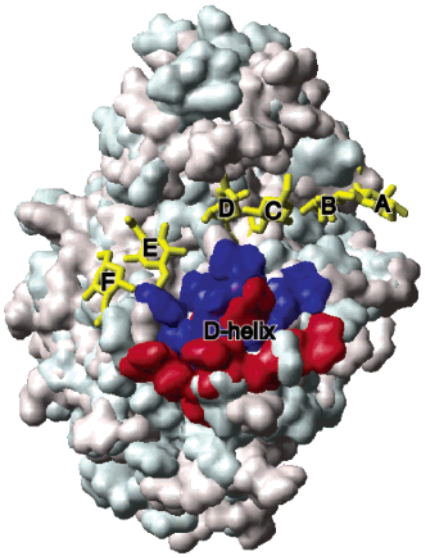

FIGURE 5: GRASP representations of the structures of human lysozyme determined at 4 and 35 °C, which are superimposed so as to minimize the rmsd between the two backbone coordinates. The large active site cleft is located between the α- and β-domains, in which the polysaccharide binding subsites denoted as A−F are indicated. The polysaccharide's sugar ring is indicated by yellow. The D-helix portion is colored in blue for 4 °C and red for 35 °C, respectively.

of the active site cleft, leading to the tight associations with the polysaccharides. The present result suggests that the closing of the active site cleft occurs at the active site lobe only by temperature lowering without any substrate. It might be possible to assume that the active site lobe of human lysozyme undergoes the "opening" and closing of the cleft as a function of the temperature, because such result was obtained in our previous NMR study on NTnC (*4*), which revealed that a functional segment comprising a "helix−loop−helix" structural unit packs more tightly against the rest of the protein with lowering of the temperature; NTnC becomes the more inactive form by the temperature lowering (*4*). It should be noted that NTnC is constructed by α-helices as the dominant secondary structural motifs, while human lysozyme comprises both α-helices and β-strands. It might be interesting that the structure of the functional domain of these two proteins commonly possesses a specific temperature dependence irrespective of their difference in principal structural constituents.

The adiabatic compressibility experiments revealed that a partial specific volume (v^0) of chicken hen egg white lysozyme decreases from 0.717 to 0.703 mL/g with lowering of the temperature from 40 to 10 °C (*5*), which was assumed to be contributed by the low-temperature-induced shrinkage of the volume of the cavity originating from imperfections in atom packing. The present study revealed that a similar decrease in total volume and accessible surface area occurs in human lysozyme (Table 3), which is indicative of the low-temperature-induced shrinkage of the internal cavity of this molecule. Indeed, it observed a slight depression of the internal motion of the backbone NH bond vector with temperature lowering (Figure 4), which will be interpreted as that the internal fluctuation space becomes small with lowering of the temperature. It should be noted that the overall molecular motional correlation time (τ_m) becomes 2-fold slower (5.2 → 12.9 ns), which will be explained by a 2-fold increase in viscosity of water. Overall, the structural changes of human lysozyme are consistent with a low-temperature-induced decrease in v^0, as proposed on the basis of compressibility experiments.

Among the members of the C-type lysozyme, only rainbow trout lysozyme was assumed to be one of the cold-adapted variants since its lytic activity is higher than that of the other lysozymes below 20 °C (*14*). The X-ray structure of this fish lysozyme was determined when it forms three complexes with the polysaccharide ligand of $(NAG)_2$, $(NAG)_3$, and $(NAG)_4$, respectively, which were compared with the ligand-free form (*12*). Interestingly, the maximum difference in atom positions between the ligand-bound and -free forms of the rainbow trout lysozyme is less than 0.3 Å (Figure 12 of ref *12*). The region that exhibits the greatest conformational change was assigned to residues from Leu^{100} to Asp^{119}, which forms the active site lobe (*12*). This 0.3 Å difference is significantly small if compared with the difference between the ligand-free and -bound forms of human lysozyme (∼1.5 Å) (Figure 1 of ref 10). In the present study, a larger than 2 Å difference in backbone atom positions was observed for the lobe region between the 4 and 35 °C structures of human lysozyme (Figure 3B). These data suggest that in rainbow trout lysozyme the active site lobe acquires less mobility compared with human lysozyme, which might be one of the key determinants to differentiate the catalytic efficiency between the two lysozymes under low temperatures. It should be noted that Trp^{109} of human lysozyme was demonstrated to be extremely important for the catalytic reaction through its van der Waals contact with Glu^{35} (*48*). Rainbow trout lysozyme contains the corresponding residues of Trp^{108} and Glu^{35}, so that a factor to define the nature of active site lobe of rainbow trout lysozyme may be ascribed to a portion including the other amino acid residues.

To summarize, we succeeded in determining the solution structures of human lysozyme at 35 and 4 °C using the conventional multidimensional NMR spectroscopy. The detailed comparison between the 35 and 4 °C structures revealed for the first time that an active site lobe has a structural ability to obstruct the polysaccharide-binding cleft only by temperature lowering without any substrate. This mechanism presumably correlates with the low-temperature-induced reduction of the lytic activity. It might be speculated from the obtained data that under nondenatured conditions a functional region of a protein specifically responds to lowering of the temperature.

REFERENCES

1. Gerday, C., Aittaleb, M., Arpigny, J. L., Baise, E., Chessa, J.-P., Garsoux, G., Petrescu, I., and Feller, G. (1997) *Biochim. Biophys. Acta 1342*, 119−131.
2. Lonhienne, T., Gerday, C., and Feller, G. (2000) *Biochim. Biophys. Acta 1543*, 1−10.
3. Sheridan, P. P., Panasik, N., Coombs, J. M., and Brenchley, J. E. (2000) *Biochim. Biophys. Acta 1543*, 417−433.
4. Tsuda, S., Miura, A., Gagné, S. M., Spyracopoulos, L., and Sykes B. D. (1999) *Biochemistry 38*, 5693−5700.
5. Gekko, K., and Hasegawa, Y. (1989) *J. Phys. Chem. 93*, 426−429.
6. Salton, M. R. J., and Ghuysen, M. J. (1959) *Biochim. Biophys. Acta 36*, 552−554.
7. Salton, M. R. J., and Ghuysen, M. J. (1960) *Biochim. Biophys. Acta 45*, 355−363.
8. Artymiuk, P. J., and Blake, C. C. F. (1981) *J. Mol. Biol. 152*, 737−762.

9. McKenzie, H. A. (1996) in *Lysozyme: Model Enzyme in Biochemistry and Biology* (Jolles, P., Ed.) pp 365−409, Academic Press, Basel, Switzerland.
10. Song, H., Inaka, K., Maenaka, K., and Matsushima, M. (1994) *J. Mol. Biol. 244*, 522−540.
11. Blake, C. C., Johnson, L. N., Mair, G. A., North, A. C., Phillips D. C., and Sarma, V. R. (1967) *Proc. R. Soc. London, Ser. B 167*, 378−388.
12. Karlsen, S., and Hough, E. (1995) *Acta Crystallogr. D51*, 962−978.
13. Vollan, V. B., Hough, E., and Karlsen, S. (1999) *Acta Crystallogr. D55*, 60−66.
14. Grinde, B., Lie, O., Poppe, T., and Salet, R. (1988) *Aquaculture 68*, 299−304.
15. Redfield, C., and Dobson, C. M. (1990) *Biochemistry 29*, 7201−7214.
16. Mine, S., Ueda, T., Hahimoto, Y., and Imoto, T. (2000) *Protein Sci. 9*, 1669−1684.
17. Ohkubo, T., Taniyama, Y., and Kikuchi, M. (1991) *J. Biochem. (Tokyo) 6*, 1022−1029.
18. Lipari, G., and Szabo, A. (1982) *J. Am. Chem. Soc. 104*, 4546−4559.
19. Lipari, G., and Szabo, A. (1982) *J. Am. Chem. Soc. 104*, 4559−4570.
20. Schwalbe, H., Grimshaw, S. B., Spencer, A., Buck, M., Boyd, J., Dobson, C. M., Redfield, C., and Smith, L. J. (2001) *Protein Sci. 10*, 677−688.
21. Oka, C., Tanaka, M., Muraki, M., Harata, K., Suzuki, K., and Jigami, Y. (1999) *Biosci. Biotechnol. Biochem. 63*, 1977−1983.
22. Kumeta, H., Kobashigawa, Y., Miura, K., Nishimiya, Y., Oka, C., Nemoto, N., Miura, A., Nitta, K., and Tsuda, S. (2002) *J. Biomol. NMR 22*, 183−184.
23. Morsky, P. (1983) *Anal. Biochem. 128*, 77−85.
24. Bax, A., Griffey, R. H., and Hawkins, B. L. (1983) *J. Magn. Reson. 55*, 301−315.
25. Palmer, A. G., III, Rance, M., and Wright, P. E. (1991) *J. Am. Chem. Soc. 113*, 4371−4380.
26. Grzesiek, A., and Bax, A. (1992) *J. Am. Chem. Soc. 114*, 6291−6292.
27. Muhandiram, D. R., and Kay, L. E. (1994) *J. Magn. Reson., B 103*, 203−216.
28. Grzesiek, A., and Bax, A. (1993) *J. Biomol. NMR 3*, 185−204.
29. Marion, D., Driscoll, P. C., Kay, L. E., Wingfield, P. T., Bax, A., Gronenborn, A. M., and Clore, G. M. (1989) *Biochemistry 28*, 6150−6156.
30. Kay, L. E., Marion, D., and Bax, A. (1989) *J. Magn. Reson. 84*, 72−84.
31. Ikura, K., Kay, L. E., Tschudin, R., and Bax, A. (1990) *J. Magn. Reson. 86*, 204−209.
32. Vuister, G. W., and Bax, A. (1993) *J. Am. Chem. Soc. 115*, 7772−7777.
33. Wishart, D. S., Bigam, C. G., Yao, J., Abildgaard, F., Dyson, H. J., Oldfield, E., Markley, J. L., and Sykes, B. D. (1995) *J. Biomol. NMR 6*, 135−140.
34. Delaglio, F., Grzesiek, S., Vuister, G. W., Zhu, G., Pfeifer, J., and Bax, A. (1995) *J. Biomol. NMR 6*, 277−293.
35. Garett, D. S., Powers, R., Gronenborn, A. M., and Clore, G. M. (1991) *J. Magn. Reson. 95*, 214−220.
36. McDonald, I. K., and Thornton, J. M. (1994) *J. Mol. Biol. 238*, 777−793.
37. Brünger, A. T. (1992) *X-PLOR Version 3.1: A System for X-ray Crystallography and NMR*, Yale University Press, New Haven, CT.
38. Laskowski, R. A., MacArthur, M. W., Moss, D. S., and Thorton, J. M. (1993) *J. Appl. Crystallogr. 26*, 283−293.
39. Kraulis, P. J. (1991) *J. Appl. Crystallogr. 24*, 946−950.
40. Merrutt, E. A., and Murphym, E. P. M. (1994) *Acta Crystallogr. D50*, 869−873.
41. Koradi, R., Billeter, M., and Wüthrich, K. (1996) *J. Mol. Graphics 14*, 29−32.
42. Kay, L. E., Torchia, D. A., and Bax, A. (1989) *Biochemistry 28*, 8972−8979.
43. Farrow, N. A., Zhang, O., Forman-Kay, J. D., and Kay, L. E. (1994) *J. Biomol. NMR 4*, 727−734.
44. Feller, G., and Gerday, C. (1997) *Cell. Mol. Life Sci. 53*, 830−841.
45. Tjandra, N., Feller, S. E., Pastor, R. W., and Bax, A. (1995) *J. Am. Chem. Soc. 117*, 12562−12566.
46. Tjandra, N., Wingfield, P., Stahl, S., and Bax, A. (1996) *J. Biomol. NMR 8*, 273−284.
47. Gagné, S. M., Tsuda, S., Spyracopoulos, L., Kay, L. E., and Sykes, B. D. (1998) *J. Mol. Biol. 278*, 667−686.
48. Muraki, M., Goda, S., Nagahora, H., and Harata, K. (1997) *Protein Sci. 6*, 473−476.

BI026730W